Paper **CFDSC2013-177**,
21st Annual Conference of the CFD Society of Canada,
Sherbrooke, Canada, May 6-9, 2013.

Numerical Simulations of Experimentally Observed High-Amplitudes, Self-Sustained Pitch-Heave Oscillations of a NACA0012 Airfoil

Jean-Christophe Veilleux and Guy Dumas[1]

Laboratoire de Mécanique des Fluides Numérique, Département de Génie Mécanique, Université Laval, Québec, G1V 0A6, Canada

Email: *jean-christophe.veilleux.1@ulaval.ca*

Abstract

A numerical model for simulating self-sustained pitch-heave oscillations of a NACA0012 airfoil undergoing coalescence flutter is developed for high Reynolds number applications. In the transitional Reynolds number regime, such oscillations have been observed experimentally and begin to be documented. The two dimensional fluid-structure model of the present study is implemented using *OpenFOAM-2.1.x*, an open-source finite volume CFD code. Numerical results obtained with simulations making use of the Spalart-Allmaras turbulence model are compared to preliminary experimental results. Laminar and SST $k-\omega$ simulations are also carried out to investigate their qualitative and quantitative effects on the results. We find that results obtained with the laminar calculations agree fairly well with experimental data for both structural heave stiffnesses investigated. Results obtained making use of the turbulence models agree well with the experiments for the cases where the airfoil's dynamics is dominated by the structural stiffness, and the match is not as good for the cases where the aerodynamic plays a more significant role on the airfoil's dynamics. Explanation for these observations is provided as well as discussion on the validation status of the proposed FSI model.

1 Introduction

The fluid-structure interaction of an airfoil with it's surrounding fluid is of great interest in the design process of several devices. In the field of aeroelasticity, much effort has been directed towards a better understanding of the flutter phenomena combined with the development of effective predictive techniques. Flutter is the result of a positive net exchange of energy from the fluid to the structure. Accurate prediction of this energy transfer is often crucial in order to avoid high amplitude structural vibrations of a system. In such cases, the relative transfer of energy from the fluid must be kept small when compared to the damping capacity of the apparatus. Conversely, airfoils undergoing flutter could be conceived as devices to harvest energy from an incoming fluid, thus transforming the flapping airfoil into some sort of turbine. In such cases, one would want the positive flux of energy from the fluid to the structure to be maximized.

Following the pioneering work of McKinney and DeLaurier [8] in the field of flapping airfoils turbines, significant research on the subject has been performed by several groups in the last decade with a general goal of optimizing the concept. Doing so, the promising potential of flapping foils as wind or hydrokinetic turbines has been confirmed both numerically [3, 4] and experimentally [5] by the authors' group. In most cases, the rigid airfoil was mounted on a clever mechanical system in which the form and relation between the pitching and heaving motions were enforced in such a way to significantly increase the efficiency of the turbine [5]. Among these systems, some involved a well designed mechanical coupling between both motions which reduced the device to a single degree of freedom. Whether one or two degrees of freedom, optimization of the energy harvester has primarily been achieved through a direct implicit or explicit control on the shape and frequency of the airfoil's motions in pitch and heave.

Recently, some research groups reported promising results concerning a simplified semi-passive version of the flapping foil power generator. In these semi-passive systems, the pitching motion of the foil is prescribed while the heave results naturally through the interaction of the foil with the flow and the supporting mechanism [18, 19]. Energy harvesting efficiencies up to 25% were reported, thus confirming the potential of this simplified mechanism. According to Zhu *et al.* [18] and to Kinsey *et al.* [3], the extraction of energy is mainly attributable to the heave motion. This means that the pitching motion produces or incurs modest input or output of energy, which suggests the concept of a further simplified fully passive system [17]. This idea that the pitching motion can be fully autonomous in an energetic sense was experimentally [14] and numerically [6] validated by observing self-sustained pitching-only motion of the airfoil at transitional Reynolds numbers.

In the simplified fully passive system, both heave and pitch are entirely determined through the fluid-structure interaction between the foil, the flow and the elastic supports. This relatively new idea offers significant mechanical advantages over the preceding mechanisms at the cost of having no direct control over the motion of the foil. Reported results from Peng *et al.* [11] with an efficiency up to 20% for a foil mounted on a rotational spring and a linear damper undergoing large amplitude cycle oscillations revealed the potential of this new form of turbine, and further optimization of this passive system is probably at reach. This optimization must be achieved by adjusting parameters of the apparatus having an indirect effect on the motion of the foil, thus implying that an adequate understanding of the physical mechanisms through which each parameter influences the motion is critical. Note here that for the purpose of turbine applications, only cases for which limit cycle oscillations (LCO) emerge are of interest. For such cases, the airfoil oscillates in a non-chaotic way with a single frequency for both motions (pitch and heave).

In the present study, the airfoil is elastically mounted on a linear spring-damper base in heave and a rotational spring-damper base in pitch. The airfoil is free to pitch and heave independently: no mechanical linking is enforced between both degrees of freedom. The resulting simplified fully passive system still offers enough adjustable parameters to suggest that an adequate indirect control of the airfoil's dynamics is possible. The main objective of this paper is to develop and validate an adequate CFD model of the problem for future works optimizing the energy extraction efficiency of this turbine concept. High Reynolds numbers being more representative of a hydrokinetic turbine application, RANS turbulence modeling is incorporated. A secondary objective of this research is also to gain preliminary physical insight into the physics at play. Limited experimental results from Mendes *et al.* [9] and Poirel *et al.* [12, 15] in the transitional Reynolds numbers regime are available for this specific setup and are thus used to compare and validate the proposed numerical approach.

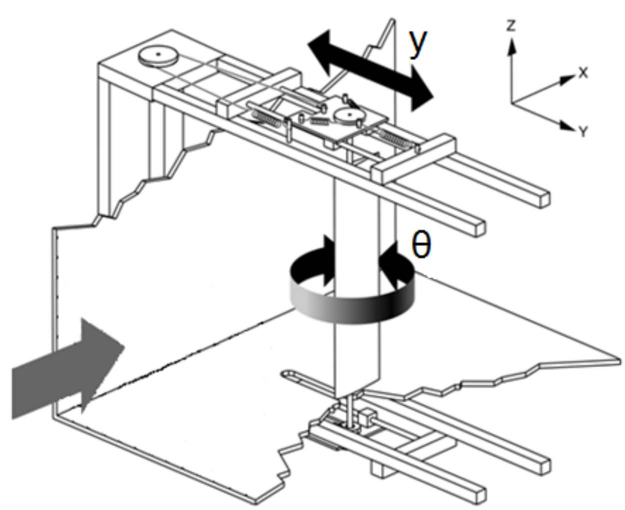

Figure 1: *Schematic of the elastically mounted airfoil. Reproduced from [13].*

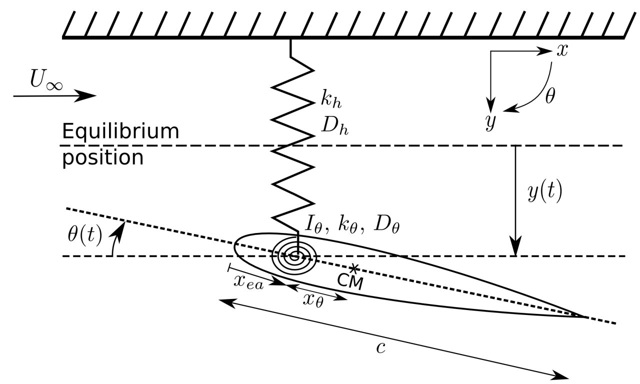

Figure 2: *Simplified schematic of the elastically mounted airfoil (not showing the sliding mechanism) with symbolic representation of key parameters. Adapted from [7].*

2 PROBLEM MODELING

2.1 Aeroelastic Modeling

In the present implementation, the elastically mounted airfoil is free to pitch around the z-axis and heave along the y-axis. The motion is not possible in any other directions nor about any other axis. As shown in Figure 1, the two degree-of-freedom system consists of a rigid airfoil mounted on a pivot about which the pitching motion (θ) is possible. Further, the pivot is mounted on a sliding mechanism thus allowing the heave motion (y). There is no mechanical linking between the pitching and heaving motions. Instantaneous aerodynamics as well as inertial effects are the only possible couplings. It is worth noting that the heaving mass (m_h) and pitching mass (m_p) of such a system do not need to be equal and this must be taken into account. One can convinced oneself by considering Figure 1 where the mass of the sliding mechanism is not involved with the pitching of the airfoil.

The general equations of motion of such a system can be derived starting with a summation of forces and moments exerted on the airfoil (see Figure 2):

$$\Sigma F_y = -\mathcal{L} - D_h \dot{y} - k_h y \ , \tag{1}$$

$$\Sigma M_z = M_{ea} - D_\theta \dot{\theta} - k_\theta \theta \ , \tag{2}$$

where $\mathcal{L}$ is the aerodynamic lift (downward positive), M_{ea} is the aerodynamic moment about the elastic axis (clockwise positive), k_h and k_θ are respectively the heave and torsional spring stiffness coefficients, D_h and D_θ are respectively the heave and torsional damping coefficients and the superscript $(\dot{\cdot})$ denotes differentiation with respect to time.

It is also necessary to relate the instantaneous linear acceleration of the airfoil at the center of mass (a_{cm}) to the instantaneous acceleration of the airfoil at the elastic axis ($a_{ea} = \ddot{y}$):

$$\vec{a}_{cm} = \vec{a}_{ea} + \ddot{\vec{\theta}} \times \vec{r}_{cm-ea} + \dot{\vec{\theta}} \times \left(\dot{\vec{\theta}} \times \vec{r}_{cm-ea} \right) , \quad (3)$$

where $\vec{r}_{cm-ea}$ is the instantaneous vector that extends from the pivot point to the center of mass of the airfoil including all rotating parts. This vector can be written using the variable x_θ defined as the distance between the pivot point and the center of mass as shown in Figure 2:

$$\vec{r}_{cm-ea} = x_\theta \cos(\theta)\, \widehat{e_i} + x_\theta \sin(\theta)\, \widehat{e_j} \ . \quad (4)$$

A simplified expression for a_{cm} can then be obtained and the vectorial notation can be dropped since the linear acceleration is solely along the y-axis:

$$a_{cm} = a_{ea} + \ddot{\theta}\, x_\theta \cos\theta - \dot{\theta}^2 x_\theta \sin\theta \ . \quad (5)$$

It must be emphasized that the instantaneous acceleration of the center of mass of the heave-only components ($m_h - m_p$) is equal to the instantaneous acceleration of the airfoil at the elastic axis (a_{ea}). One can convince oneself of this by substituting $x_\theta = 0$ in Eq. (5). In heave, it is possible to write the summation of forces along the y-axis as the sum of forces acting on both the pitching and non-pitching components separately:

$$\Sigma F_y = \{(m_h - m_p)\, a_{ea}\} + \{m_p\, a_{cm}\} \ . \quad (6)$$

Combining Eqs. (1), (3) and (6), yields the final result:

$$-\mathcal{L} = m_h \ddot{y} + m_p \left(\ddot{\theta} x_\theta \cos\theta - \dot{\theta}^2 x_\theta \sin\theta \right) + D_h \dot{y} + k_h y \ . \quad (7)$$

The equation of motion in pitch can be derived in a more straightforward way since the heave-only components do not need to be considered in the analysis. The summation of moments exerted on the airfoil can be written as:

$$\Sigma \vec{M}_z = I_\theta \ddot{\vec{\theta}} + \vec{r}_{cm-ea} \times m_p\, \vec{a}_{ae} \ , \quad (8)$$

where I_θ is the moment of inertia about the elastic axis. Using Eq. (4) in the right-hand side and using Eq. (2) in the left hand side, the following result is obtained after dropping the vectorial notation since all terms are along the z-axis:

$$M_{ae} = I_\theta \ddot{\theta} + m_p \ddot{y} x_\theta \cos\theta + D_\theta \dot{\theta} + k_\theta \theta \ . \quad (9)$$

2.2 Computational Modeling

The aeroelastic problem is solved using *OpenFOAM-2.1.x* [10], a finite volume open-source CFD code. The fluid flow around the airfoil is assumed incompressible and viscous at moderate to high Reynolds numbers. Further, volume forces are neglected. Thus the governing equations of the 2D flow are the mass and momentum conservation equations obtained with the Reynold's decomposition, here expressed using the Einstein notation:

$$\frac{\partial U_i}{\partial x_i} = 0 \ , \quad (10)$$

$$\frac{\partial U_i}{\partial t} + U_j \frac{\partial U_i}{\partial x_j} = -\frac{1}{\rho} \frac{\partial p}{\partial x_i} + (\nu + \nu_t) \frac{\partial^2 U_i}{\partial x_j^2} \ , \quad (11)$$

where ν_t is the turbulent kinematic viscosity provided by the Spalart-Allmaras turbulence model unless otherwise indicated. The PISO segregated algorithm is used in order to efficiently couple pressure and velocity, resulting in a significant reduction of computation time over a SIMPLE algorithm. The transient term is discretized using a second order backward implicit scheme. The convective term is discretized using a second order scheme based on a linear upwind interpolation. The diffusive term finally is discretized using a second order scheme based on a linear interpolation and uses an explicit non-orthogonal-limited surface normal gradient scheme. The linear solver is a generalized geometric-algebraic multigrid (GAMG) method for both the pressure and momentum equations and a smooth solver using Gauss-Seidel methods is used for the turbulence equation.

The flow solver must be coupled with the dynamics of the airfoil in order to predict fully and accurately the present fluid-structure interaction. This is achieved by using an algorithm that performs the following calculations at each time step:

1. The external fluid flow is computed;
2. The instantaneous forces and moment exerted by the flow on the airfoil are computed;
3. The equations of motion are solved and the new airfoil positions and velocities are updated;
4. The calculation continues to the next time step.

In all simulations, unless otherwise noted, a time step providing a minimum of 3000 steps per oscillatory cycle and 200 steps per convective time unit is used according to the following equation:

$$\Delta T = \min \left\{ \frac{1}{3000\, f} \ , \ \frac{c}{200\, U_\infty} \right\} \ , \quad (12)$$

where f is the frequency of oscillation, c is the chord length and U_∞ is the freestream velocity. Validation of this time step size is presented in §3. Further, a RMS convergence criterion of 1×10^{-5} is enforced on pressure residuals, while the criterion is 1×10^{-6} for momentum and turbulence.

The pitching and heaving airfoil problem is here solved in a non-inertial frame of reference. The translational motion of the airfoil is taken into account by the usage of a momentum source term and unsteady boundary conditions on the velocity. The pitching motion requires moving body and moving grid capabilities.

Dynamic mesh capabilities are included in *OpenFOAM*. A non-conformal sliding interface is used in this work to take into account the pitching motion of the solid body. This strategy avoids deforming meshes or remeshing techniques, which could considerably slow down the calculation. As shown in Figure 3, the central circular portion of the mesh is free to rotate around the z-axis. This dynamic grid has a radius of exactly two chords while the entire grid covers a domain of 100 × 100 chords. At the interface, an interpolation scheme is required and this is achieved by using the native *OpenFOAM* Arbitrary Mesh Interface (AMI) [1]. This dynamic mesh technique was validated in the past by Kinsey *et al.* [3] and Lapointe *et al.* [6] and the accuracy of the method was thoroughly confirmed.

The computational domain is shown in Figure 3. A time-varying but uniform velocity is prescribed at all 3 inlet planes while a constant mean static pressure is prescribed at the outlet. Varying inlet velocities are required to take into account the instantaneous heaving motion of the airfoil. Further, a viscosity ratio of $\nu_t/\nu = 1$ is set at all inlets to correspond to negligeable turbulence upstream of the airfoil.

The 2D mesh shown is built with approximately 65 000 cells, having close to 450 points on the airfoil to provide enough near-body resolution and capture sufficiently the physics of the flow. The first cell thickness is set in order to obtain $y^+ \approx 1$ on the airfoil surface throughout the simulations for all incoming flow velocities considered. It must be clear that the mesh used for the simulations is the same at all flow velocities, meaning that the first cell thickness was chosen relative to the most restrictive case considered here (Re=120 000).

In all cases, the simulations are initialized with a perturbed airfoil by specifying an initial heaving velocity ($\dot{y}_0$). All other initial values are set to zero, namely $y_0 = 0$, $\theta_0 = 0$ and $\dot{\theta}_0 = 0$. The parameter $\dot{y}_0$ is set to approximately 5-10% of U_∞. This allows the transient period to be shortened to approximately 10 to 25 cycles, depending mainly on the freestream velocity. Other parameters of the apparatus also influence the duration of the transient regime and care must be taken in order to reduce computation time. The typical runtime for a whole simulation is about 75 hours on eight Intel Nehalem-EP processors.

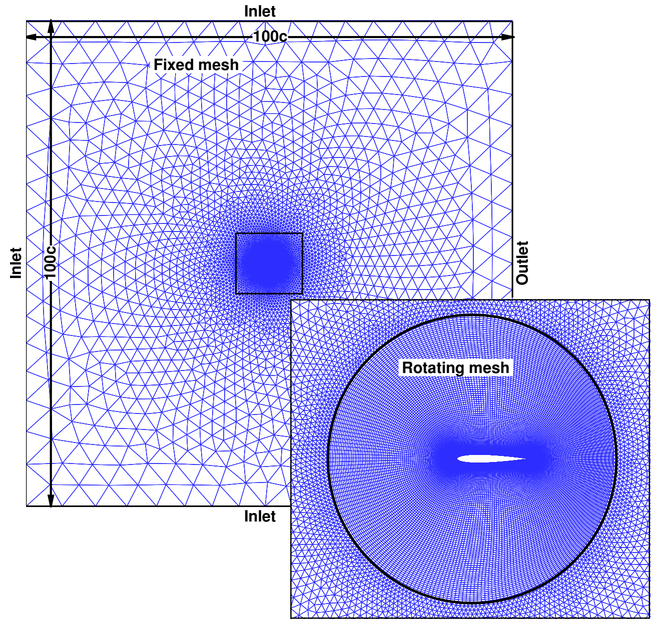

Figure 3: *Computational domain and grid details (≈ 65 000 cells).*

2.3 Turbulence Modeling

In this study, turbulence closure is achieved by the Boussinesq eddy-viscosity approximation. The eddy viscosity ν_t is calculated using the Spalart-Allmaras (SA) RANS model. The latter is a one equation turbulence model for the modified turbulent viscosity $\tilde{\nu}$. The model used is the version originally presented by the authors in 1994 [16].

Previous works at the LMFN such as [7] and [2] on pitch-heave oscillations of an airfoil validated the use of the SA turbulence model for this purpose. They found that although this model does not always provide excellent quantitative agreement with experimental data, the qualitative results and the trends are typically fairly good. The SA model was developed based on aerodynamics considerations of stationary bodies. As for any RANS model, great care must be taken when massive separation is encountered and the reader must keep in mind the usual limitations of RANS simulations. It is recalled that this study is for the moment primarily concerned with the general trends of the physical responses. For this specific purpose, RANS simulations are justified.

In this paper, limited laminar computations (no turbulence model) and SST k-ω computations have also been performed for comparison with results obtained with SA. In the case of SST k-ω, various inlet's turbulence intensity have been used and very little changes were observed for an increase or decrease of one order of magnitude of the inlets' turbulence intensity. A fairly low inlet turbulence intensity of approximately 0.2% has finally been retained for the calculations.

Time step	C_L (%)	C_M (%)	C_p (%)
Coarse	0.72	4.23	2.62
Baseline	–	–	–
Fine	0.01	0.22	0.96

Table 1: *Maximum variation over one complete cycle of oscillation for different time steps.*

Mesh	C_L (%)	C_M (%)	C_p (%)
Coarse	0.78	4.35	6.60
Baseline	–	–	–
Fine	0.57	2.70	5.02

Table 2: *Maximum variation over one complete cycle of oscillation for different grids.*

3 Numerical Validation

Time step size independence was demonstrated by varying the time step from the baseline value used throughout the simulations. A fine time step providing 26 000 steps per cycle of oscillation and 2400 steps per convective time unit did not affect noticeably the results. Variations of less than 0.25% were observed on the amplitudes of oscillation (θ_{max} and y_{max}). A coarser time step providing 500 steps per cycle of oscillation and 50 steps per convective time unit was also investigated. Variations of 0.5% were observed on the amplitudes of oscillation. The maximum variation on the lift coefficient (C_L), on the moment coefficient (C_M) and on the power coefficient (C_p) are shown in Table 1.

For the RMS convergence criterion, refinement of one order of magnitude compared to the baseline case previously described in §2 did not significantly affect any of the parameters recorded. A similar conclusion is drawn for a criterion coarser by an order of magnitude. It could be justified to use the coarser values although this idea was not retained in this paper.

Mesh validation was achieved with a run on a coarse grid of approximately 30 000 cells (250 points on the airfoil) and a run on a refined grid of approximately 120 000 cells (650 points on the airfoil). For the refined grid, differences of less than 1% were observed on the recorded amplitudes of motion while the observed differences are closer to 2% for the coarser grid. More results are presented in Table 2. We conclude that the baseline mesh provides enough resolution for the intended purpose of this paper.

At last, since all computations have been run in parallel on 8 cores, the results of a serial computation were compared to those of a parallel computation (8 cores). All quantities checked matched nearly perfectly.

Parameter	Value
c	0.156 m
x_{ea}	0.186 c
x_θ	0.095 c
I_θ	0.00135 kg·m^2
k_θ	0.3 N·m/rad
D_θ	0.002 N·s/rad
m_h	2.5 kg
m_p	0.77 kg

Table 3: *Fixed parameters of the experimental apparatus from Poirel and Mendes [15, 12, 9]*

.

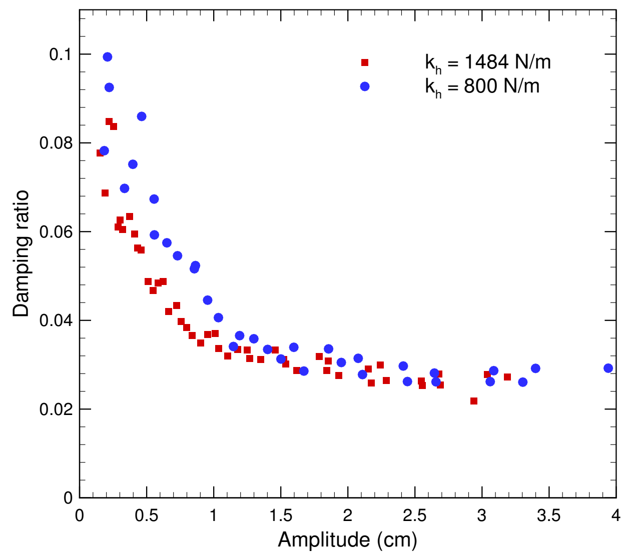

Figure 4: *Evolution of the damping ratio in heave as a function of the maximum cyclic amplitude (from experimental data of [12]).*

4 Results

Experimental results from Mendes *et al.* [9] and Poirel *et al.* [15, 12] in the transitional Reynolds number regime are available for the setup previously described. The specific parameters indicated in Table 3 are relative to the experimental setup used at the RMC in Kingston. Results are available for a large and a low heave stiffness, respectively $k_h = 1484$ N/m and $k_h = 800$ N/m. Based on free-decay experimental tests, the damping ratio in heave of the apparatus behaves in a highly non-linear way as shown in Figure 4. The damping ratios on this figure were calculated using the logarithmic decrement method and are based on the response of the airfoil during a no-flow, free-decay test for which the pitch angle was blocked at $\theta = 0$ deg. Raw data of the free decay tests were provided by Prof. Poirel [12].

For the sake of this paper, the damping ratio in heave is considered to be constant and equal to the asymptotic value for large amplitudes, which yields a damping coefficient $D_h = 2$ Ns/m associated to a damping ratio of 0.0225. This hypothesis can be revisited and discussed *a posteriori* once the heaving amplitudes of the resulting oscillations are known.

4.1 Large Heave Stiffness

With the aforementioned parameters, numerical simulations have been performed for freestream inlet velocities similar to those of the wind tunnel ranging from 4.68 m/s (Re = 50 000) to 11.23 m/s (Re = 120 000). Experimental and numerical results for a large heave stiffness are gathered on Figures 5 and 6. As one can see, the match between experimental and numerical frequencies is excellent for all simulations. A single oscillatory frequency emerges for this 2DOF apparatus. This is explained by the specific type of flutter observed, which is due to the coalescence of both pitching and heaving aeroelastic modal frequencies [9, 15]. The amplitudes of oscillation resulting from this dynamic instability grow exponentially untill structural forces or non-linear aerodynamic obstruct the growth and make LCO appear.

Experimentally and numerically, the apparatus oscillates at a frequency nearly identical to the calculated structural natural frequency in heave. It is clear that the airfoil's motion is heave dominated in this configuration. Furthermore, the near overlap of the structural natural frequency and the LCO frequency indicates that the aerodynamics plays a minor role in heave, it's effect being dominated by the structural stiffness of the apparatus. This does not imply unsignificant aerodynamic forces and moments, but suggests that the airfoil's motion is mainly driven by the linear springs in heave.

Indeed, the aerodynamic stiffening is significant on the rotational motion of the airfoil. It accounts for the coalescence of the oscillatory frequencies. Outside of the experimental range, the predicted frequencies suggest that these conclusions still hold true. The structural stiffness being dominant for this specific configuration of the apparatus justifies the label "large heave stiffness" previously attributed.

As shown in Figure 6, the amplitudes of the predicted geometric pitching angle θ compares well with the observed amplitudes over the limited experimental range. Error bars are displayed on the laminar results as a way to quantify the fluctuations of the predicted amplitudes from one cycle to the other. The average amplitude is therefore displayed with error bars extending up to the maximum and minimum amplitudes recorded. Results obtained with both turbulence models predicted constant amplitudes once the transitory period was terminated, typically after 10 to 25 cycles.

Laminar simulations predict amplitudes slightly lower or equal to those predicted with the SA turbulence model. It must be noted that the differences increase as the Reynolds number grows. The same can be said relative to the heaving amplitude. Unfortunately, the experimental uncertainties over the results and over the apparatus' parameters were not addressed in the referred works.

4.2 Low Heave Stiffness

For the case of a low heave stiffness, the experimental and numerical data are shown on Figures 7, 8 and 9. Note here that the effective angle of attack α_{eff} is used instead of the geometric angle θ to quantify the pitching amplitude. This is indeed required for comparison with experimental data for which the geometric angle was not provided. The effective angle of attack is calculated as:

$$\alpha_{eff} = \theta + \arctan(\dot{y}/U_\infty) \tag{13}$$

Results of simulations performed by the authors based on the work from Lapointe *et al.* [7] are also included to better illustrate the significant effect of using unequal masses in heave and pitch. The trends of the results based on the work from Lapointe *et al.* (labeled as $m_h = m_p$) are clearly contrasting from the experimental results' trends. The model from Lapointe *et al.* [7] failed to match the results from Mendes and Poirel [9] since it lacked the flexibility of setting different heaving and pitching masses. The results obtained using this model would be accurate for actual equal masses in pitch and heave which is not the case with the RMC's setup.

The quite different trends obtained with $m_p = m_h$ are attributable to the inertial coupling between pitching and heaving associated with the elastic axis being offset from the heaving center of mass. As a result, a vertical acceleration induces a moment on the airfoil. Further, a pitching motion or a rotational acceleration may induce a vertical force on the airfoil. As can be seen in Eqs. (7) and (9), these forces and moments are proportional to the *pitching* mass. A model lacking the ability to set m_p and m_h independently would therefore always set these forces to be proportional to the *heaving* mass, thus overpredicting the inertial coupling. Having two distinct masses in heave and pitch clearly provides one more way to control the dynamics of the airfoil for future optimizations.

Present results making use of distinct heaving and pitching masses compare well in frequency to the experimental results. For the simulations making use of the SA turbulence model, the match is excellent in the lower range of Reynolds numbers, and a slight discrepancy appears with growing Reynolds number. The predicted amplitudes of the effective angle of attack with SA show a trend which agrees well with the experiment up to Re = 80 000 although all predicted values are fairly low. As observed for the larger heave stiffness, the

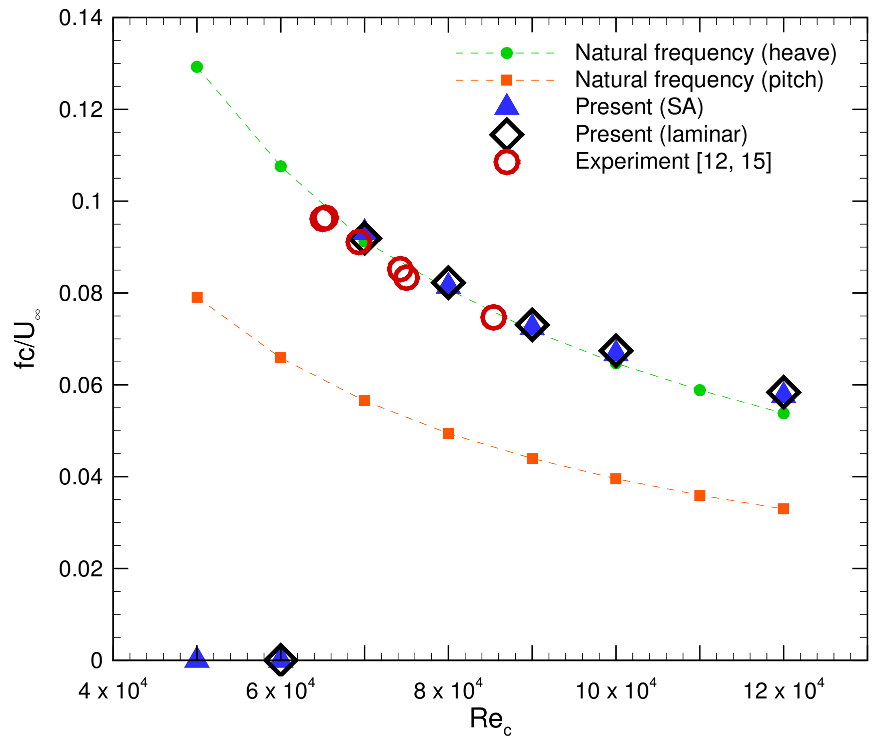

Figure 5: *Predicted frequencies compared to experimental measurements and calculated natural structural frequencies (large heave stiffness k_h = 1484 N/m).*

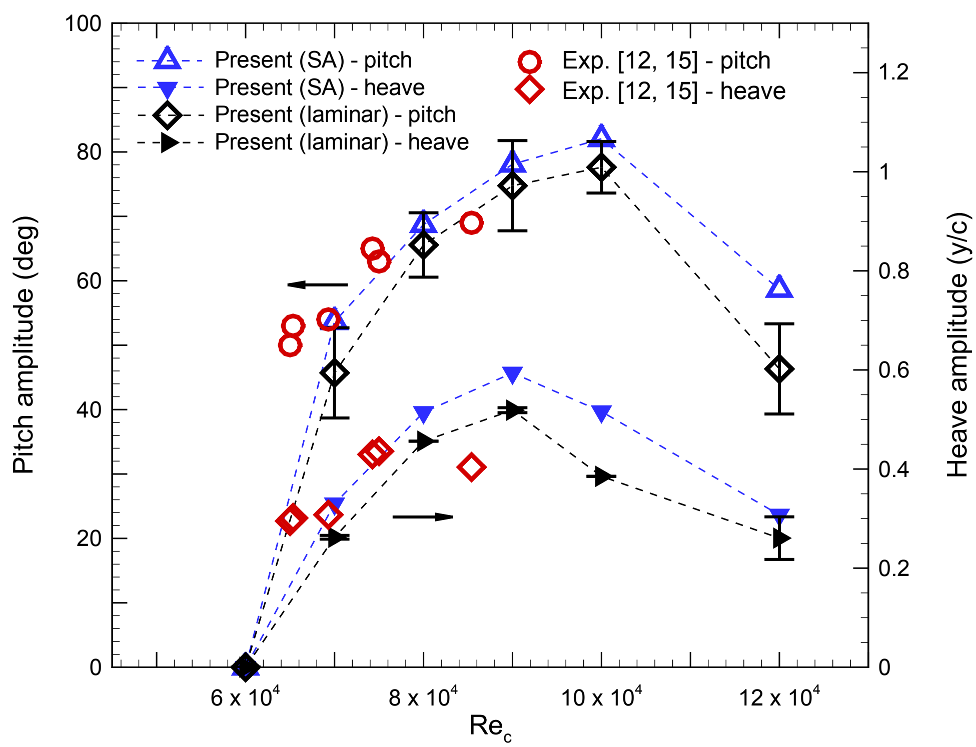

Figure 6: *Predicted pitch and heave amplitudes compared to experimental data (large heave stiffness k_h = 1484 N/m). Error bars on the laminar results show the range of variation of the oscillation amplitudes from cycle to cycle.*

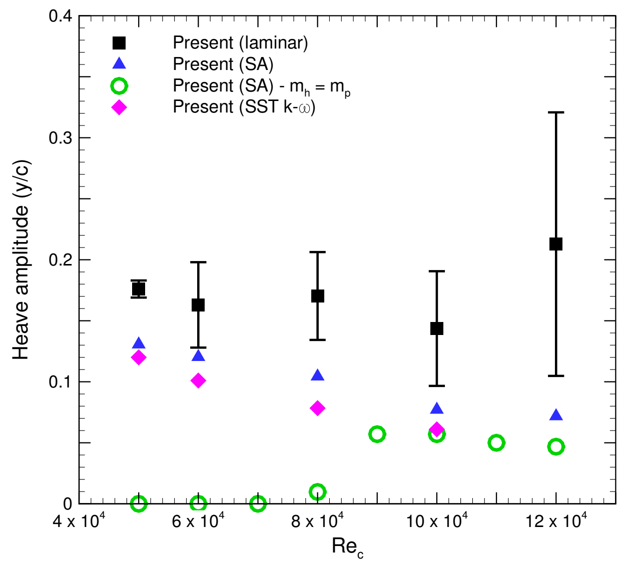

Figure 7: *Predicted heave amplitudes (k_h = 800 N/m). No experimental data available. Error bars on the laminar results show the range of variation of the oscillation amplitudes from cycle to cycle.*

trend becomes different from the experimental results as the Reynolds number is increased. The same conclusions can be drawn relative to the simulations performed with the SST k-ω turbulence model. Actual results also suggest that the greatest differences between results predicted by both turbulence models are for the higher range of Reynolds numbers. None provides a qualitative nor quantitative agreement with experimental results better than the other.

Further simulations with different damping coefficients in heave and pitch indicate that the uncertainties relative to these parameters (associated to the non-linear behavior of the experimental damping) does not fully account for the mismatches. Variations of the heaving damping coefficient within a range that still allows sustained oscillations did not prove to have a significant effect on the oscillatory frequency as shown on Figure 10. Note that the label *strong damping* refers to $D_h = 3.5$ Ns/m. Conversely, the maximum effective angle of attack exhibits some variations following a change of the damping coefficient in heave as shown in Figure 11, but, again, cannot explain the mismatch alone. A simulation with no structural damping showed that the predicted amplitudes remain well below the experimental values for most of the considered Reynolds numbers range. This strongly suggests that the uncertainties over the heave damping do not account for the low predicted amplitudes. Further, it appears that a variation of the damping coefficient has an impact which is smaller with an increase of the Reynolds number.

In counterpart, laminar simulations display a behavior more representative of the experimental results. The predicted frequencies agree very well with the experiments. The predicted amplitudes of the effective angle of attack are much more representative of the experimental values and are generally higher that those predicted with the SA turbulence model.

The match with experimental results being well improved by a laminar calculation suggests that the turbulence model fails at predicting important features of the flow, probably because it produces too much turbulent viscosity in the higher range of Reynolds numbers. This could explain the growing discrepancy in the trend of the results obtained with SA as the Reynolds number is increased. This idea is confirmed by an analysis of the ν_t/ν contours close to the airfoil. As shown in Figure 12, the ratio of turbulent viscosity in the attached boundary layer on the upper side is much higher than one would expect, especially for Re = 120 000. Contours of vorticity are displayed on Figure 13. The vorticity field is found to be very different for a laminar simulation than with the SA turbulence model. The effective body is considerably thinner for the laminar simulation. The Reynolds number also has a significant effect on the vorticity field, but comparison is more difficult since the dynamics of the airfoil is also modified with the Reynolds number.

For this low heave stiffness, the experimental and numerically predicted oscillation frequencies are found to be distinct from both the pitching and heaving natural frequencies. Aerodynamic stiffening is therefore present and active both in pitch and in heave. This suggests that the aerodynamics is far more dominant here than it was with the large heave stiffness case. Further, the fluctuations of predicted amplitudes with laminar simulations being greater with the low heave stiffness case suggests the same conclusion. This could partially explain why the turbulence model has a more significant effect with a low heave stiffness. If the motion is dominated by the structural stiffness, discrepancy in the prediction of the flow features has a weaker impact.

5 CONCLUSION

A numerical model for simulating self-sustained pitch-heave oscillations of an airfoil undergoing coalescence flutter was developed and put to the test. In the range of transitional Reynolds numbers, laminar results display a behavior more representative of the experimental results than would be predicted with the SA or SST $k-\omega$ turbulence model, especially for the case where the aerodynamics is dominant. This suggests that the model could be improved by making use of a transitional turbulence model more appropriate to the flow regime considered. On the other hand, the developed model displays a behavior which provides enough confidence that it could adequately be used at higher Reynolds numbers more representative of a hydrokinetic turbine, which is the intended

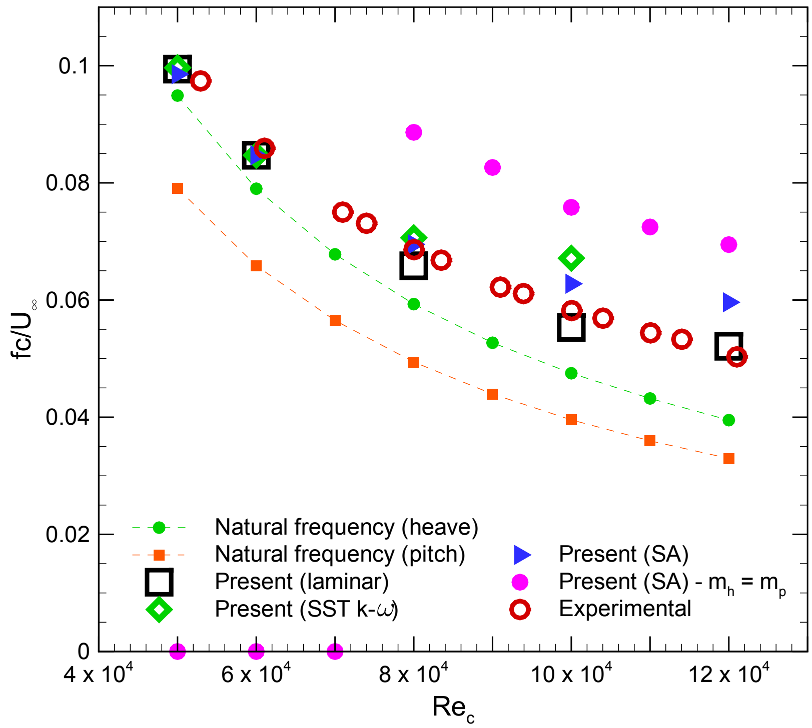

Figure 8: *Predicted frequencies compared to experimental measurements and calculated natural structural frequencies (k_h = 800 N/m).*

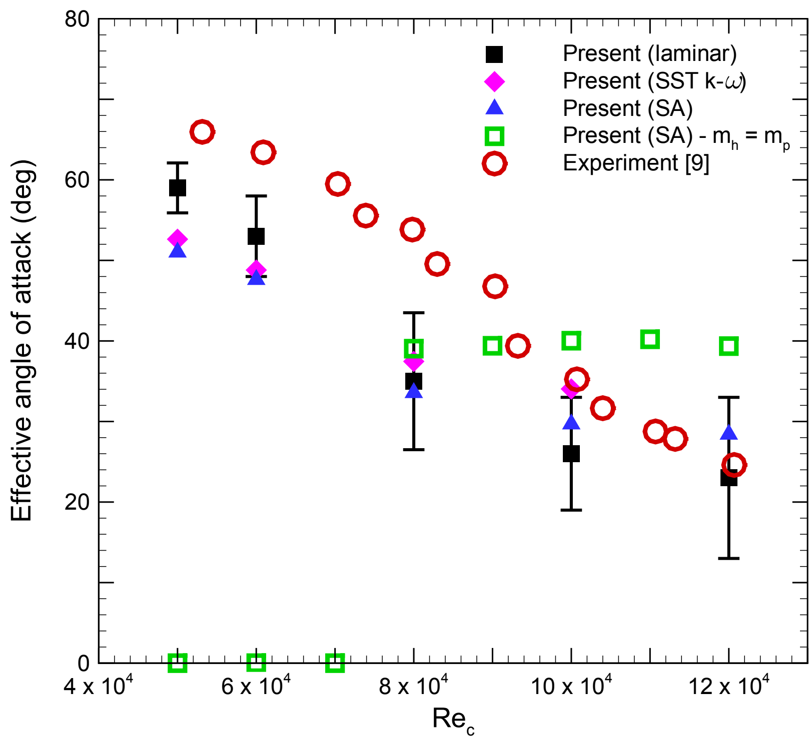

Figure 9: *Predicted effective angles of attack compared to experimental measurements (k_h = 800 N/m). Error bars on the laminar results show the range of variation of the oscillation amplitudes from cycle to cycle.*

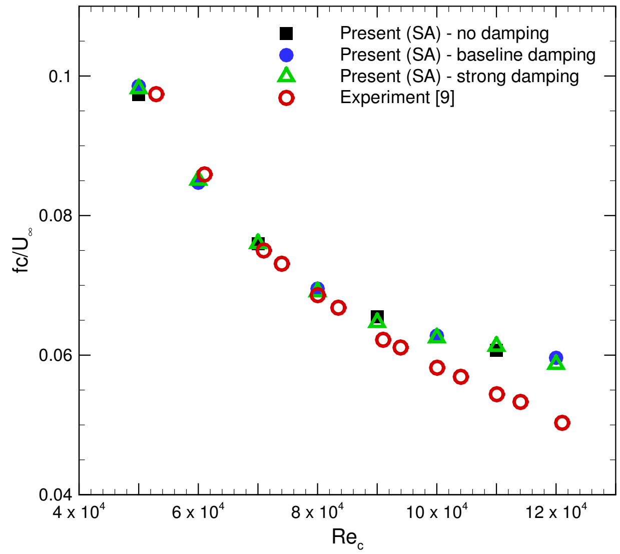

Figure 10: *Effect of the modulation of the heaving damping on the oscillatory frequency (k_h = 800 N/m).*

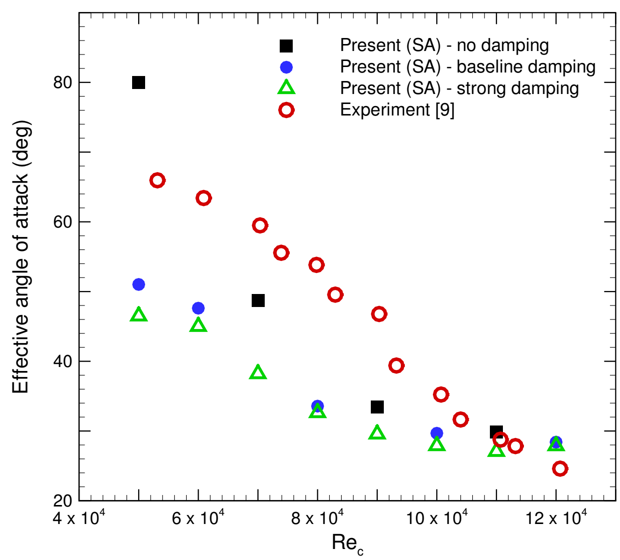

Figure 11: *Effect of the modulation of the heaving damping on the effective angle of attack's amplitude (k_h = 800 N/m).*

purpose in a near future. Further optimization could also be achieved with a modulation of the damping coefficients representative of the apparatus simulated to account for the non-linearities observed on the set-up. This would also require the viscous damping to be subtracted from the measured total damping in order to obtain a good estimation of the structural damping alone as a function of the amplitude of oscillation.

ACKNOWLEDGEMENTS

Computations were performed on the Colosse supercomputer at the CLUMEQ HPC Consortium under the auspices of Compute Canada. The authors would also like to thank Prof. D. Poirel for acces to his experimental results and S. Lapointe for his expert help with OpenFOAM. Financial support from NSERC/DG program is also gratefully acknowledged.

REFERENCES

[1] P. E. Farrell and J. R. Maddison. Conservative interpolation between volume meshes by local Galerkin projection. *Computer Methods in Applied Mechanics and Engineering*, 200(1-4):89–100, 2011.

[2] S. Julien, G. Dumas, and V. Métivier. URANS simulations of high amplitude flapping airfoils. Toronto, Canada, May 2007. 15th Annual Conference of the CFD Society of Canada. Paper CFD-2007-1117.

[3] T. Kinsey and G. Dumas. Parametric study of an oscillating airfoil in a power-extraction regime. *AIAA Journal*, 46(6):1318–1330, 2008.

[4] T. Kinsey and G. Dumas. Computational fluid dynamics analysis of a hydrokinetic turbine based on oscillating hydrofoils. *Journal of Fluids Engineering, Transactions of the ASME*, 134(2), 2012.

[5] T. Kinsey, G. Dumas, G. Lalande, J. Ruel, A. Mehut, P. Viarouge, J. Lemay, and Y. Jean. Prototype testing of a hydrokinetic turbine based on oscillating hydrofoils. *Renewable Energy*, 36(6):1710–1718, 2011.

[6] S. Lapointe and G. Dumas. Improved numerical simulations of self-sustained oscillations of a NACA0012 with transition modeling. Honolulu, HI, June 2011. 41st AIAA Fluid Dynamics Conference. Paper AIAA-2011-3528.

[7] S. Lapointe and G. Dumas. Numerical simulations of self-sustained pitch-heave oscillations of a NACA0012 airfoil. Canmore, Alberta, 2012. CFD Society of Canada.

[8] W. McKinney and J. DeLaurier. Wingmill: An oscillating-wing windmill. *AIAA Paper 80-0621R*, pages 80–87, 1980.

[9] F. Mendes, D. Poirel, and A. Benaissa. Experimental investigation of self-sustained pitch-heave aeroelastic oscillations of a NACA0012 airfoil at transitional Reynolds numbers. Montreal, Canada, January 2011. CASI2011.

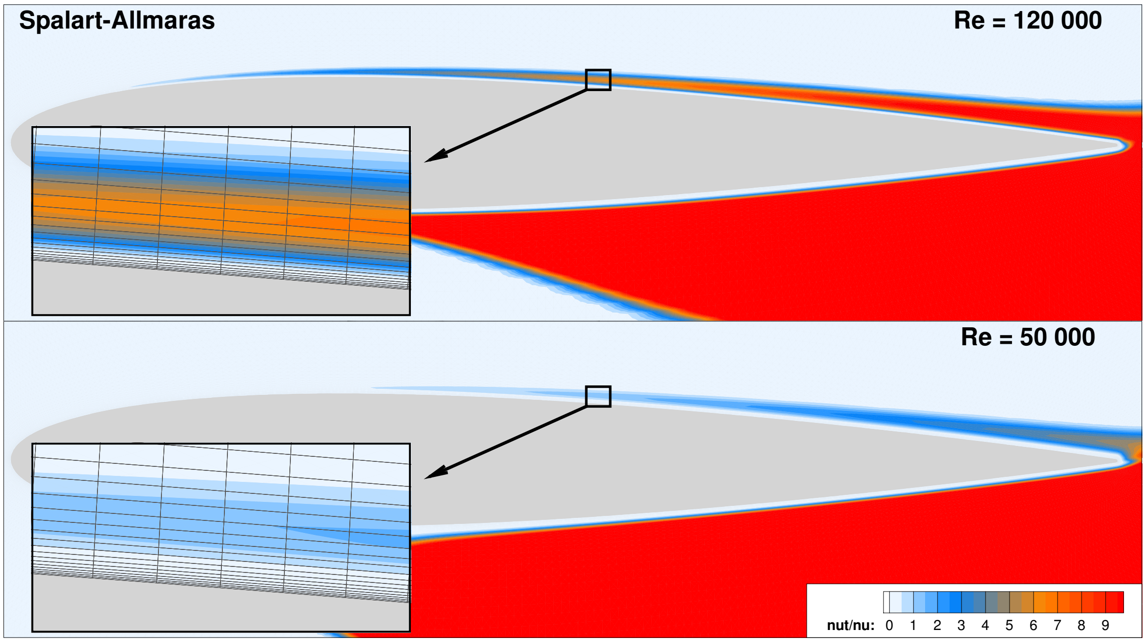

Figure 12: *Close up view on the instantaneous turbulent viscosity ratio ν_t/ν for Re = 120 000 and Re = 50 000.*

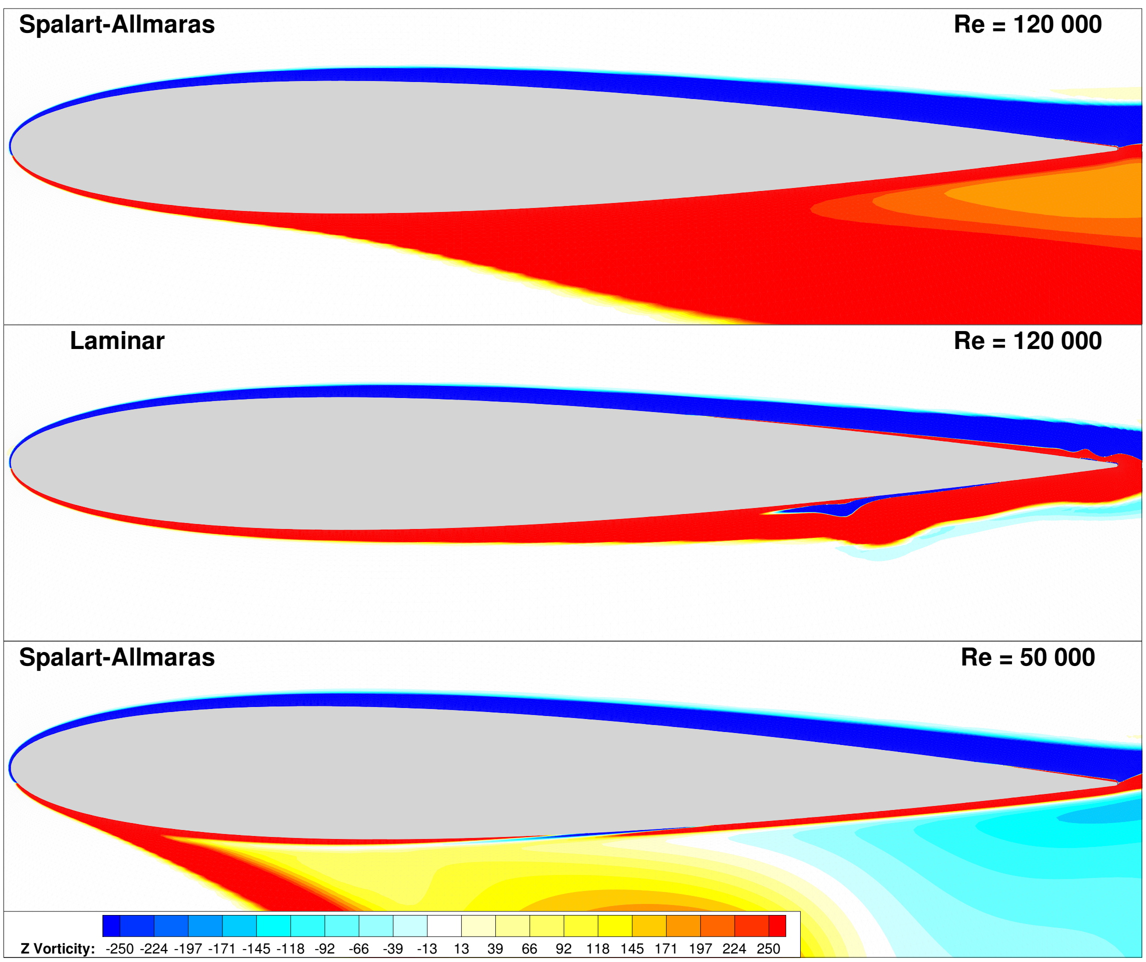

Figure 13: *Comparison of instantaneous vorticity contours for Re = 120 000 and Re = 50 000.*

[10] OpenCFD. *OpenFOAM - The Open Source CFD Toolbox - User's Guide*. OpenCFD Ltd., United Kingdom, 2.1 edition, May 2012.

[11] Z. Peng and Q. Zhu. Energy harvesting through flow-induced oscillations of a foil. *Physics of Fluids*, 21(12):1–9, 2009.

[12] D. Poirel. personal communication, July 2012.

[13] D. Poirel, Y. Harris, and A. Benaissa. Aeroelastic dynamics of a NACA 0012 airfoil in the transitional Reynolds number regime. Vancouver, Canada, July 2006. ASME PVP.

[14] D. Poirel, Y. Harris, and A. Benaissa. Self-sustained aeroelastic oscillations of a NACA0012 airfoil at low-to-moderate Reynolds numbers. *Journal of Fluids and Structures*, 24(5):700–719, 2008.

[15] D. Poirel and F. Mendes. Experimental investigation of small amplitude self-sustained pitch-heave oscillations of a NACA0012 airfoil at transitional Reynolds numbers. Nashville, TN, January 2011. AIAA Aerospace and Science Meeting.

[16] P. R. Spalart and S. R. Allmaras. One-equation turbulence model for aerodynamic flows. *Recherche aerospatiale*, (1):5–21, 1994.

[17] Q. Zhu. Optimal frequency for flow energy harvesting of a flapping foil. *Journal of Fluid Mechanics*, 675:495–517, 2011.

[18] Q. Zhu, M. Haase, and C. H. Wu. Modeling the capacity of a novel flow-energy harvester. *Applied Mathematical Modelling*, 33(5):2207–2217, 2009.

[19] Q. Zhu and Z. Peng. Mode coupling and flow energy harvesting by a flapping foil. *Physics of Fluids*, 21(3):033601, 2009.